LWT - Food Science and Technology 253 (2026) 119660

Contents lists available at ScienceDirect

LWT

journal homepage: www.elsevier.com/locate/lwt

Molecular and structural characterization of food emulsions by combination of multiple advanced imaging techniques

Peter Sjövall [a,*], Annika Altskär [b], Niklas Lorén [b]

[a] RISE Research Institutes of Sweden, Brinellgatan 4, 50462, Borås, Sweden
[b] RISE Research Institutes of Sweden, Frans Perssons väg 6, 41276, Gothenburg, Sweden

A B S T R A C T

Food emulsions are complex colloidal systems whose structural and molecular properties critically influence stability and sensory attributes. This study combines cryogenic time-of-flight secondary ion mass spectrometry (cryo-ToF-SIMS) with transmission electron microscopy (TEM) and confocal laser scanning microscopy (CLSM) to characterize the chemical and structural properties of bovine milk, cream, and an oat-based cream analogue. Cryo-ToF-SIMS enabled parallel mapping and spatial correlation of multiple molecular components, including fat, proteins, calcium, phospholipids and sugars, in microscopic structures, such as fat globules and interstitial elongated aggregates, which were structurally characterized at the nanometer level with TEM. ToF-SIMS correlation analysis revealed significant differences in the molecular composition of the interstitial aggregates, with considerably less mixing of components in the oat-based cream analogue. In addition, 3D analysis of individual milk fat globules generated depth profiles of calcium and proteins at the surface of fat globules, consistent with casein binding to the surface of the protein-containing milk fat globule membrane (MFGM). Furthermore, the triglyceride content of the fat globules were characterized using mass spectra from ToF-SIMS and found to be consistent with the reported fatty acid distributions in Swedish cow milk for bovine milk and cream, and in rapeseed oil for oat-based cream analogue.

1. Introduction

Food emulsions are complex colloidal systems where two immiscible liquids, typically oil and water, are mixed to form a stable dispersion. Detailed chemical and microstructural knowledge of these emulsions is important for the food industry, as they provide essential properties such as texture, mouthfeel, taste, and stability in a wide range of products including dressings, sauces, and beverages (Tan & McClements, 2021).

Molecular interactions at the micrometre and nanometer length scales are critical for the stability and sensory properties of food emulsions (McClements, 2015; Ravera et al., 2021), e.g., by influencing the size distribution of the fat droplets (dispersed phase), the viscosity of the continuous phase, and the type and concentration of emulsifiers/-stabilizers at the interfaces between the dispersed and continuous phases, as these factors affect the likelihood of coalescence and phase separation leading to creaming, flocculation, or sedimentation. However, current methods for molecular/structural characterization of food emulsions are limited in the nature and detail of information that they can provide (Kupikowska-Stobba et al., 2024). Confocal laser scanning microscopy (CLSM) is a powerful method for imaging the distribution of various components in emulsions at spatial resolutions down to the sub-micrometre range, using fluorescent stains for molecular specificity. Structures in the nanometer range in emulsions can be imaged by transmission electron microscopy (TEM), following cryo-based sample preparation procedures. In this manuscript, a novel analytical approach, based on *in situ* mass spectrometry imaging, for the study of food emulsions is presented. Its potential together with TEM and CLSM to provide structural and molecular information at superior spatial resolution and molecular specificity compared to conventional methods is demonstrated.

Time-of-flight secondary ion mass spectrometry (ToF-SIMS) is an imaging mass spectrometry method capable of molecular imaging of solid surfaces at lateral resolutions down to 0.1-1 μm (Jia et al., 2023). The analysis is extremely surface sensitive, with only the top ca. 1 nm of the sample surface being probed, but 3D information can be obtained by combining the 2D imaging analysis with sputter etching, which gradually removes material from the sample surface in a highly controlled and homogeneous manner. The method has been used to obtain 3D distributions of specific molecular compounds/structures in biological samples, including cells (Brison et al., 2013), biofilms (Zhang et al., 2020) and human skin (Sjovall et al., 2024; Starr et al., 2022), but not yet in food emulsions. However, as the analysis is carried out in vacuum, freezing of the sample using cryo-preparation protocols and analysis under cryogenic conditions are required. Furthermore, quantification

* Corresponding author.
E-mail address: peter.sjovall@ri.se (P. Sjövall).

https://doi.org/10.1016/j.lwt.2026.119660
Received 18 February 2026; Received in revised form 18 June 2026; Accepted 22 June 2026
Available online 22 June 2026

with ToF-SIMS is complicated by matrix effects, and the sensitivity and selectivity can be highly variable for different analytes, which also affect the 3D imaging capacity. Some key analytical properties are compared in Supplementary Table S1 for the three imaging methods used in this work.

Bovine milk and cream are natural oil-in-water emulsions, with fat droplets dispersed in an aqueous phase rich in proteins, lactose, and minerals. The two main fractions of the milk proteins, casein micelles (about 80%) and whey proteins (20%) (Lara-Villoslada et al., 2005), both act as primary emulsifying agents. Due to their amphiphilic structure, casein micelles and whey proteins form a protective layer around fat droplets, preventing coalescence and phase separation (Zhou et al., 2022). The lipid content in bovine milk is dominated by triglycerides (97-98 wt% (German & Dillard, 2006),), with a minor fraction of phospholipids (0.2-1 wt%).

Oat-based milk and cream analogues are oil-in-water emulsions (Lapcikova et al., 2024) that are stabilized by oat-derived components such as beta-glucans, proteins, and starches. Beta-glucans, a type of soluble fiber found in oats, play a crucial role in stabilizing these emulsions (Li et al., 2019). The fat component in these emulsions is mainly rapeseed oil that is added during processing. As for all plant-based dairy products, the development of stable emulsions with the desired sensory attributes is a challenging task due to the variety of added components and processing parameters that need to be selected and optimized. An improved understanding of the structural properties and molecular interactions in these emulsions would potentially facilitate such product development and considerably benefit the food industry.

In this work, cryo ToF-SIMS is combined with TEM and CLSM to characterize the spatial distributions of molecular components in milk, cream, and oat-based cream analogues (Supplementary Fig. S1). Special consideration is given to the novel analytical opportunities provided by ToF-SIMS, including 3D imaging and spatial correlation of multiple emulsion components, as well as molecular characterisation of specific structures by *in situ* mass spectrometry. The overall aim is to investigate how the combination of ToF-SIMS, TEM and CLSM may allow for improved chemical and structural analysis of emulsion interfaces at high spatial resolution, which is important for increased understanding of the stability and sensory properties of emulsions.

2. Materials and methods

2.1. Samples

Bovine milk (Arla, färsk mjölk, 3% fat) and cream (ICA/Skånemejerier, matlagningsgrädde, 13% fat), as well as an oat-based cream analogue (Oatly, iMat, 13% fat) were purchased from local supermarkets. The content of nutrients (per 100 g) for the three samples, given by the manufacturers on their websites, is provided in Table 1. The milk was pasteurized at 72-74 °C for 15 s (high-temperature short-time (HTST) pasteurization) and the cream at about 140 °C for 2-5 s (ultra-high temperature (UHT) pasteurization). The oat-based cream analogue was pasteurized at 140 °C for 10 s (using UHT). Pasteurization and other processing techniques influence the properties of the emulsions in different ways, e.g., heating of milk has been found to induce the formation of complexes of whey proteins and casein (Rabbani et al., 2025; Yu et al., 2023).

Table 1
Nutrition contents of the three samples, according to the manufacturer's websites.

Ingredient	Bovine Milk (g per 100 ml)	Bovine Cream (g per 100 ml)	Oat-based Cream Analogue (g per 100 ml)
Total fat	3	13	13
- **saturated fat**	1.9	8.3	1.6
Total carbohydrates	4.6	4.1	6.2
- **sugar**	4.6	4.1	3.0
Proteins	3.5	3.1	0.9
Salt	0.09	0.08	0.11

2.2. Time-of-flight secondary ion mass spectrometry, ToF-SIMS

In ToF-SIMS, high-energy (primary) ions in a focused beam collide with the sample surface, causing the emission of (secondary) ions that are detected in a time-of-flight mass analyser to produce a mass spectrum from the top ca. 1 nm of the sample surface (Supplementary Fig. S1). By scanning the primary ion beam across a selected analysis area, spatially resolved mass spectrometry data are collected and can be presented, e.g., as ion images, showing the signal intensity of specific secondary ions over the analysis area, or mass spectra from selected regions of interest (ROIs) within the analysis area. Quantification using ToF-SIMS is complicated by the fact that the ion yield (signal intensity) is not only proportional to the surface concentration, but also dependent on the chemical environment of the analyte, so-called matrix effects, which add uncertainties and typically exclude absolute quantification entirely. Furthermore, the ion yield can be highly variable between different ions and analytes, which (without calibration) prohibits the use of signal intensities for comparing the abundance of different analytes in a measurement. With these limitations, ToF-SIMS is frequently used to compare the relative concentration of specific molecular species between samples or between different areas of the same sample.

The samples were prepared by depositing a 4 µl droplet of the emulsion sample onto a freshly cleaved mica sheet, placing another mica sheet on top of the droplet and plunge-freezing the entire "sandwich" sample in liquid nitrogen. The frozen sample "sandwich" was mounted on the pre-cooled ToF-SIMS sample holder while keeping it cold inside a container partially filled with liquid nitrogen. The sample holder was then quickly transferred into the sample load lock of the ToF-SIMS instrument, removing the top mica sheet immediately prior to closing, for evacuation and transfer into the analysis chamber. The sample temperature was kept below −100 °C during the entire transfer process and at ca. −160 °C during the ToF-SIMS analyses.

The ToF-SIMS analyses were performed in an M6 instrument (IONTOF GmbH, Münster, Germany) using 30 keV Bi_3^+ primary ions and low-energy electron flooding for charge compensation. Prior to analysis, the sample surface was subjected to sputter etching using 10 keV Ar_{2000}^+ ions (typically 600 × 600 µm^2, 9.8 nA, 190 s), to remove condensed ice and the topmost part of the frozen emulsion sample (possibly subject to molecular surface gradient effects). The analyses were carried out with the instrument in the delayed extraction mode to obtain both high mass ($m/\Delta m \approx 5000$) and high lateral ($\Delta L \approx 300$ nm) resolution. Data were acquired over analysis areas of 60 × 60 µm^2 to 300 × 300 µm^2 with 1024 x 1024 pixels in analysis-sputter cycles, alternating one frame of analysis (105 s, pulsed current 0.05 pA) and 5 frames of sputter etch (7.3 s per cycle, 600 × 600 µm^2, 6.5 nA). Assuming a typical sputter yield of 40 nm^3 (Seah, 2015), the sputter rate was about 4.5 nm/s and the total sputter depth during measurements was 660-990 nm (20-30 cycles). After acquisition, minor drift in the instrument was compensated for by the "shift correction" function in the instrument software (SurfaceLab 7.5, IONTOF GmbH). Ion images were generated by adding signal intensities of ions representing the same molecular component, as specified in Supplementary Table S2. When needed, the images were subjected to binning and/or reduction of the maximum intensity of the colour scale, to improve the visibility of the measured distributions. Depth profiles were extracted from manually selected ROIs of individual fat globules and displayed as average signal intensity of two consecutive data points. ROIs for measurements of the diacyl glycerol (DAG) and fatty acid distributions were generated from the fat images using the threshold selection function of the instrument software. For comparison of the Ca/protein signal intensity ratio in the milk ion images, ROIs were

selected from the $C_xH_y^+$ and K^+ ion images, to represent fat globules and the interstitial network, respectively, using the threshold selection function of the instrument software.

Data were acquired in positive and negative ion mode, however, mainly positive ion data are presented here. Three positive ion measurements from randomly selected analysis areas were conducted from one preparation of each sample.

For quantification of the colocalization of components, Pearson Correlation Coefficients (PCC) were calculated from the ToF-SIMS images (binned to 256x256 pixels) using the formula

$$r = \frac{\sum ((R_i - R_{av}) \times (G_i - G_{av}))}{\sqrt{\sum (R_i - R_{av})^2 \times \sum (G_i - G_{av})^2}} \quad (1)$$

where R_i and G_i are the signal intensities of components R and G in pixel i and R_{av} and G_{av} are the average signal intensities of components R and G in the entire image (Adler & Parmryd, 2010).

Furthermore, scatter plots of pairwise molecular components were generated using the ToF-SIMS instrument software (SurfaceLab 7.5, IONTOF GmbH).

2.3. Transmission electron microscopy, TEM

In transmission electron microscopy (TEM), a high-energy electron beam is transmitted through an ultrathin specimen, and an image is generated based on differences in the density of the sample. In the bright-field mode, structures with higher density, e.g., heavier atoms or high-density crystal structures, appear darker in the image. A sensitive CMOS camera enables analysis of low-contrast structures at low electron doses, without the need to enhance contrast by staining with heavy metals.

At least two replicates of each emulsion sample were prepared for TEM analysis by freeze substitution, plastic embedding, and thin sectioning. Freeze substitution minimizes ultrastructure artifacts by combining chemical and physical fixation (freezing) (Parlanti & Cappello, 2022). Rapid freezing is crucial to prevent ice crystal formation that can destroy the structure (Zuber & Lucic, 2019); typical signs of freeze damage are empty spaces that are surrounded by elongated structures. Here, mica sandwich for ToF-SIMS, freeze substitution and plunge freezing for TEM, and CLSM in the native state have been used to examine the microstructures. Thin films of the emulsion samples were captured with a thin wire loop (maximum of 1.5 mm^2, wire diameter approximately 150 μm) and rapidly frozen in their native state in liquid ethane/propane. The frozen film was transferred to the freeze-substitution chamber (AFS2 FSP, Leica Microsystems, Wetzlar, Germany) kept at −90 °C. The freeze substitution process was initiated by fixation of the emulsion structures using uranyl acetate in acetone with 2% anhydrous glutaraldehyde at −90 °C, followed by exchange of the water in the sample with acetone at −45 °C and then by ethanol, prior to infiltration with Lowicryl HM20 (EMS, Hatfield, PA, United States). The Lowicryl HM20 resin was polymerized at −45 °C using UV light. Ultrathin sections, around 60 nm, were cut with a Powertome XL ultramicrotome (RMC Products, Boeckeler Instruments Inc, Tucson, Arizona, United States) using a Diatome ultra diamond knife (Diatome, Hatfield, PA, United States). The sections were placed on 200 mesh TEM grids with carbon support film and analyzed in a JEM-2100Plus TEM instrument (JEOL Ltd., Tokyo, Japan) at an accelerating voltage of 200 kV with a LaB6 filament and using a CMOS camera TemCam-XF416 (TVIPS, Amtsgericht München, Germany).

2.4. Cryo TEM

Milk was analyzed using cryo-TEM to visualize casein micelles in the milk. Milk was diluted 1:3 with deionized water and plunge frozen in liquid ethane/propane using a Leica GP2 (Leica Microsystems, Wetzlar, Germany) and a TEM grid with a holey carbon film. Casein micelles are relatively stable structures and are not expected to be influenced by dilution (Horne, 2020). A droplet of the diluted milk was placed on a TEM grid with a holey carbon film. The excess liquid was blotted with filter paper to form a thin liquid film in the holes of the film. The grid was then rapidly plunged into liquid ethane to vitrify the liquid film, forming an amorphous ice film. Vitrification requires cooling rates of approximately 10^5 K/s. The TEM grid with the vitrified emulsion sample was then transferred to a pre-cooled cryo-TEM specimen holder under liquid-nitrogen conditions and inserted into the pre-cooled TEM instrument (JEM-2100Plus, JEOL Ltd., Tokyo, Japan). The analysis was carried out at an accelerating voltage of 200 kV with a LaB6 filament and using a CMOS camera TemCam-XF416 (TVIPS, Amtsgericht München, Germany) in cryo mode.

2.5. Confocal laser scanning microscopy, CLSM

The emulsions were placed in metal cups and stained with Bodipy™ FL C16 (Invitrogen) for fat and Texas Red™ sulfonyl chloride (Invitrogen) for protein and polysaccharides. The stains, dissolved in methanol and ethanol, were allowed to dry on a cover glass and then placed on top of the emulsions, enabling the stains to dissolve and diffuse into the emulsion and bind to the corresponding molecular structures. At least two replicates of each emulsion sample were examined in a Leica SP5 II CLSM instrument (Leica Microsystems, Germany). Bodipy ™ FL C16 was excited by a 488 nm laser, and the emission was recorded at 496-560 nm (shown as green in the images), whereas Texas Red ™ sulfonyl chloride was excited by a 594 nm laser, and the emission was recorded at 605-680 nm (shown as red in the images). Images with 1024x1024 pixels were acquired using a HCX PL APO 63x/1.3 glyc corr CS objective, at a scan frequency of 700-1400 Hz.

3. Results and discussion

3.1. Spatial distributions of emulsion components by ToF-SIMS

The ToF-SIMS mass spectra of all emulsion samples were dominated by peaks corresponding to water cluster ions, $H(H_2O)_n^+$, in the entire mass region up to and over m/z 600, consistent with the high water content of the emulsions (Fig. 1). Secondary ions representing other molecular components were observed at lower intensities, including hydrocarbon fragment ions representing aliphatic chains mainly present in the triglycerides of the fat globules, nitrogen-containing fragment ions characteristic of proteins and phospholipids, respectively, and intact disaccharide ions (Supplementary Table S2). Furthermore, inorganic ions were detected, including calcium and potassium.

The lateral distributions of the emulsion components are displayed in ion images, which show the added signal intensity of ions representing each component across the selected analysis area (Figs. 2–3). For all samples, water provides a relatively homogeneous background onto which the other components are localized with varying distributions (additional contrast in the water and total ion images is related to surface topography likely formed during the freeze-fraction step of the sample preparation).

Different types of structures with varying colocalization characteristics can be observed in the ion images (Fig. 3a). Furthermore, colocalization of selected components was quantitatively evaluated by calculating Pearson Correlation Coefficients (PCC) (Adler & Parmryd, 2010) for the corresponding ion images, demonstrating significant differences between the samples (Fig. 3b). In addition, scatter plots visualized correlations between selected components in specific types of structures in the ion images, also demonstrating characteristic differences between the samples (Supplementary Figs. S2–S5).

For milk, fat is entirely localized in circular structures, from <1 μm to 3-4 μm in diameter, consistent with spherical fat globules (Jukkola & Rojas, 2017), whereas the other components, i.e., calcium, proteins, disaccharide, phospholipids, and potassium are mainly colocalized in an

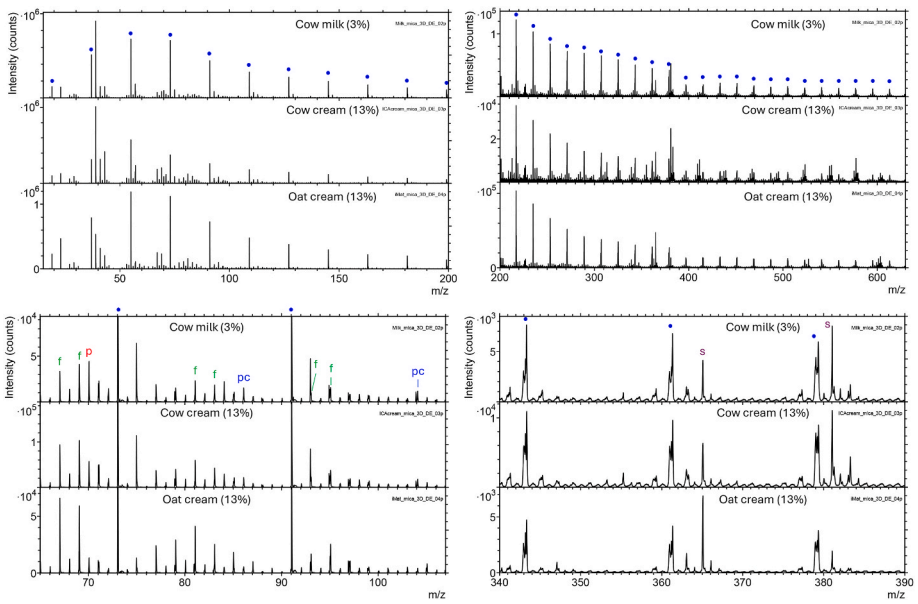

Fig. 1. Positive ion ToF-SIMS mass spectra of milk, cream and oat-based cream analogue acquired under cryogenic conditions. The panels show different m/z ranges, for display of peaks that represent the emulsion components, see Supplementary Table S2 for ion assignments. Blue dots indicate water cluster peaks, f – fat, p – proteins, pc – phosphocholine, s – disaccharide.

interstitial, network-like structure between the fat globules that consists of a mixture of elongated, thin structures (up to 20 μm long and <1 μm thick) and small spots (Figs. 2 and 3a, and Supplementary Figs. S2 and S5). Proteins are also clearly present in the fat globules (Fig. 3a). Given that the calcium content in milk is primarily bound in casein micelles and that casein is the dominant protein in bovine milk (about 80%), colocalization of calcium and proteins in the interstitial network structure indicates that casein is an abundant protein in this structure. In contrast, reduced Ca/protein signal intensity ratios in the fat globules (Fig. 3c) indicate other types of proteins associated with the milk fat globules, possibly incorporated in the milk fat globule membrane (MFGM), which is known to provide a protective layer around fat globules in human and bovine milk (O'Callaghan, McCarthy, & Carey, 2025). However, see below (Section 3.3) for the detection of calcium on the globule surfaces.

For bovine cream, fat is present in circular structures (as for milk), consistent with fat globules, but also in elongated structures, where fat is variably colocalized with the other components (Figs. 2 and 3a, and Supplementary Figs. S3 and S5). The presence of fat in elongated structures, and its partial colocalization with calcium and lactose, is different from milk, where fat was only localized to spherical fat globules. Furthermore, the elongated structures between fat globules in cream are shorter and thicker than the elongated structures in milk, and the dot-like structures in the interstitial network of milk are absent in cream.

The emulsion components of the oat-based cream analogue are quite differently distributed compared to bovine milk and cream (Figs. 2 and 3a, and Supplementary Figs. S4 and S5). Firstly, fat globules are not clearly observed, as fat is distributed in elongated, branching structures of varying shape and size. Secondly, the distribution of proteins is characterized by high signal intensities from relatively large, irregularly shaped aggregates, in combination with lower intensities from the elongated structures. Thirdly, the various components are more separated in the oat-based cream analogue compared to milk and cream, indicating less mixing. In particular, protein, fat, and disaccharide (here, likely maltose) are largely separated in the combined ion image (Fig. 3a), even within the same elongated structures, and the scatter plots display considerably less correlation between components as compared to milk and cream (Supplementary Fig. S5).

3.2. Spatial distributions of emulsion components by CLSM

A comparison of molecular images from ToF-SIMS and CLSM, showing proteins in red and fat in green, is presented in Fig. 4 for the three samples. There is a general agreement between the two methods, e.g., regarding the distribution of fat in fat globules in bovine milk and cream, and the observation of protein aggregates in the oat-based cream analogue. In addition, small fat globules mixed with proteins can be observed between the larger fat globules in the CLSM image of cream at high magnification (Fig. 4, bottom row), which suggests that the elongated structures in the corresponding ToF-SIMS image, in fact, consist of a mixture of casein, lactose and small fat globules (unresolved in the ToF-SIMS image). However, the interstitial network and elongated structures separated by water in the ToF-SIMS images are not evident in the CLSM images, where the space between fat globules is instead partly filled with proteins/polysaccharides.

We mainly attribute the difference between the CLSM and ToF-SIMS images in the space between fat globules to differences in depth resolution between the two methods. The depth resolution for CLSM under the current conditions was estimated to about 0.65 μm using the formulas described in (Pawley, 2006), whereas the ToF-SIMS image consists of a sum of images, each with a depth resolution of ~1 nm, acquired over a sputter erosion depth of around 630 nm. Despite the apparent similarity in the depths of information, the surface sensitivity of ToF-SIMS excludes contributions to the signal intensity from outside the sputter depth of 630 nm, while the depth resolution in CLSM is defined as the Full Width at Half Maximum (FWHM) of a Gaussian distribution, thus allowing for considerable intensity contributions outside the 0.65 μm depth range.

3.3. 3D information and depth profiles of emulsion components by ToF-SIMS

As most measurements were carried out with parallel sputter erosion, 3D information about the emulsion components can be extracted from the acquired data, as demonstrated, e.g., in Fig. 5a, which compares ion images of fat globules in milk, extracted from the beginning (red) and end (green) of a measurement, respectively. Here, globules present on or near the original surface (red) and globules

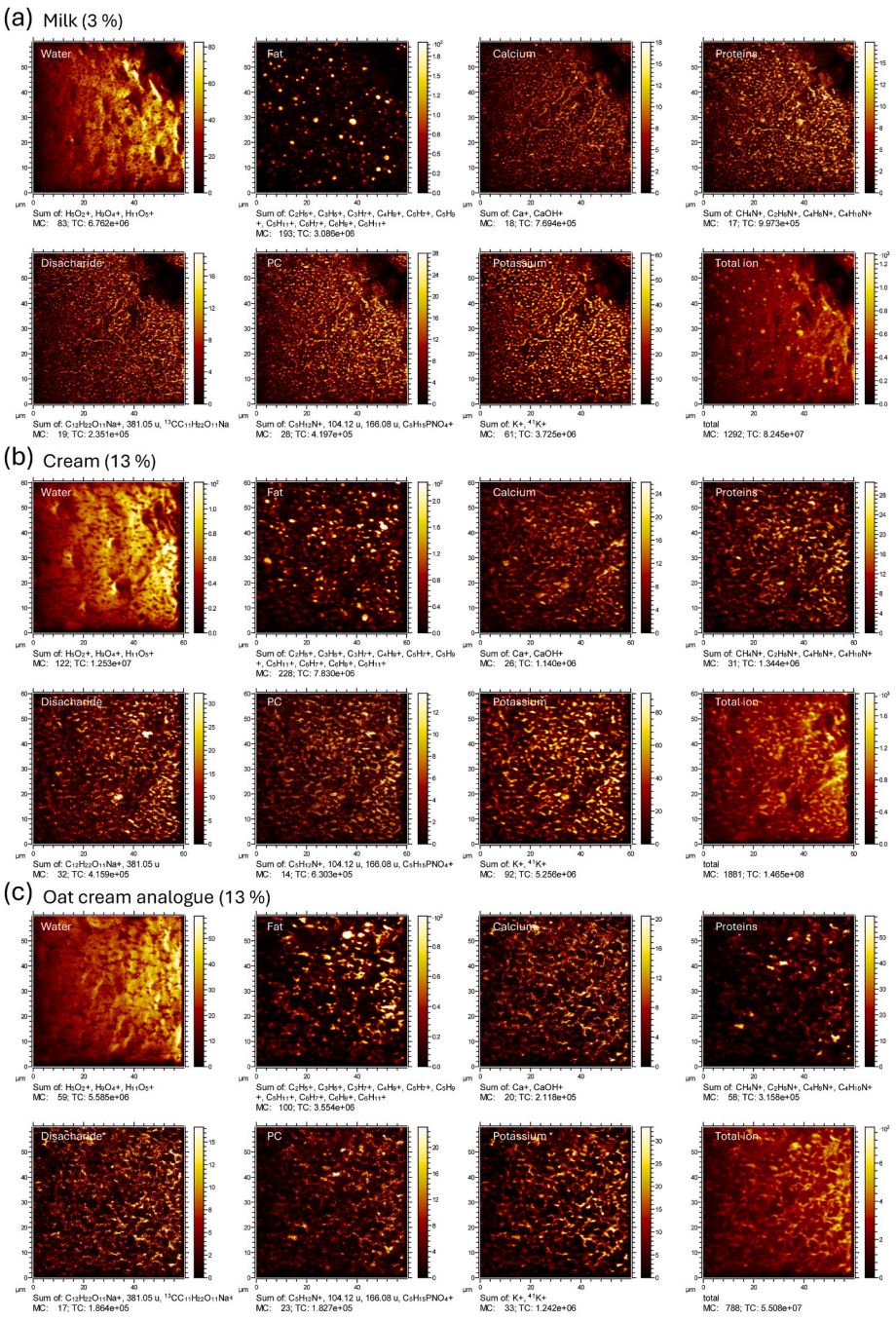

Fig. 2. Positive ion images representing various molecular components in (a) milk, (b) cream and (c) oat-based cream analogue. Field of view 60 x 60 μm^2.

located deeper into the sample (green) are clearly distinguished. Furthermore, depth profiles display the distribution of fat, proteins, and calcium at the interface between the aqueous phase and individual fat globules (Fig. 5b). Here, the elevated calcium and protein signals at the surface of the fat globule (represented by the steep increase/decrease of the fat signal) indicates binding of casein to the fat globule surface. In contrast, variably enhanced protein signals also inside the fat globules indicate the presence of proteins other than casein below the surface of the fat globules (consistent with the reduced Ca/protein ratio in the fat globules observed in Fig. 3c), presumably associated with the MFGM. However, quantitative estimates of the calcium and protein concentrations around the fat globule surface requires further measurements with additional statistical evaluation.

Furthermore, depth profiles of single fat globules in milk may be used to determine the sputter yield of this mainly aqueous sample, thereby providing a depth scale (in nm) for the 3D measurements (Fig. 6). Assuming spherical shape of the fat globules and estimating the diameters from the ion image, the sputter yield was estimated from the depth profiles of two milk fat globules to about 40 nm^3 and 50 nm^3, respectively, where the difference is attributed to possible deviations from the spherical shape and uncertainties in the diameter estimates (Fig. 6c) due to the limited lateral resolution of the ToF-SIMS measurement. Thus, our results indicate a sputter yield for the frozen milk surface that is similar to that reported previously for various polymers (Seah, 2015), thereby confirming that the sputter rate of 4.5 nm/s, used above for sample depth estimates, is a reasonable assumption for the emulsion samples in this study.

While the estimated sputter yield for the frozen milk sample provides

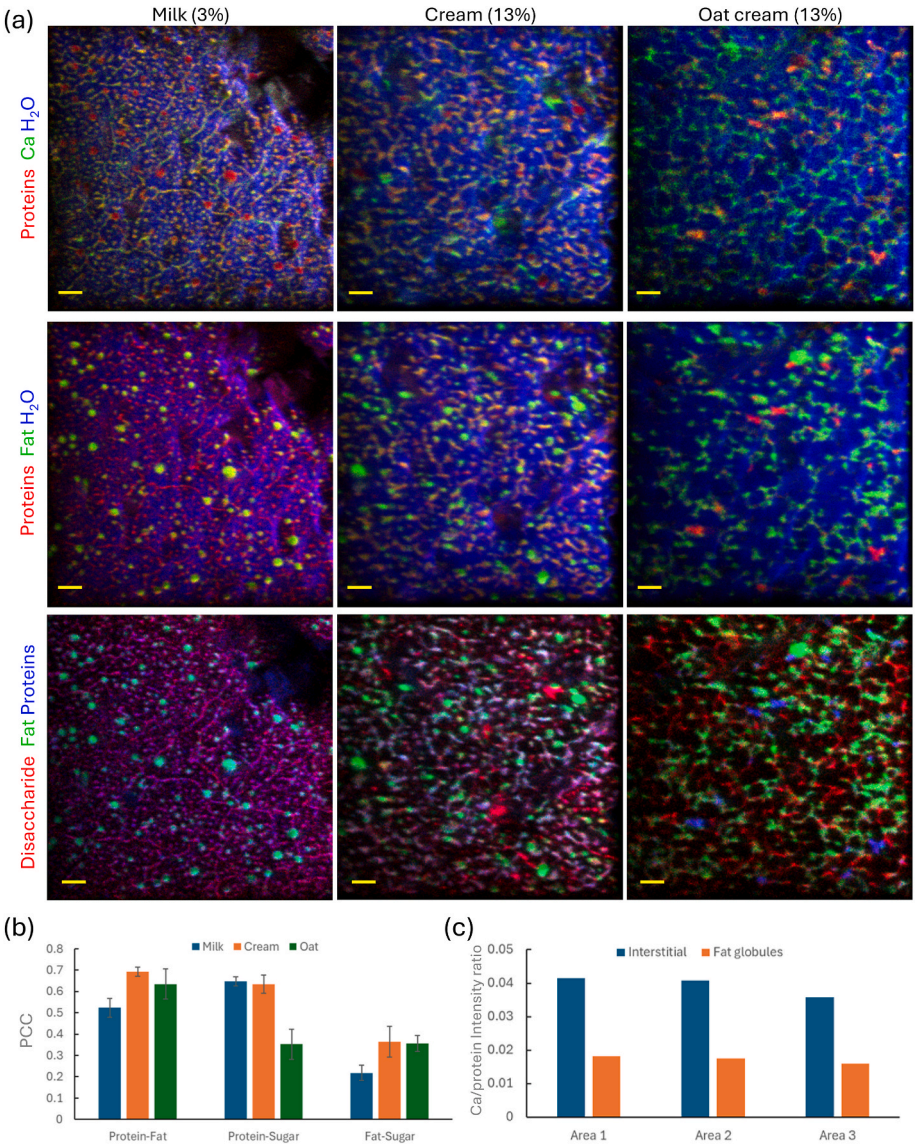

Fig. 3. Distribution and colocalization of various components in milk, cream and oat-based cream analogue. (a) 3-colour overlay ToF-SIMS ion images, (b) Pearson Correlation Coefficients, where 1 corresponds to perfect correlation, −1 to perfect anti-correlation, and 0 to complete lack of correlation, and (c) Ca/protein signal intensity ratio in fat globules versus interstitial network structures, respectively, of milk from three measurements. Scale bars in (a) are 5 μm.

valuable information for the cryo 3D analysis of other aqueous samples using Ar cluster sputtering, such as biological cells or tissues, biofilms or other emulsions, the heterogeneous nature of the sample needs to be considered for its interpretation, i.e., does the measured sputter yield represent the frozen water or the triglycerides of the fat globules, respectively? The largely symmetrical shape of the depth profiles (Fig. 6b) may provide an indication of similar sputter yields for these materials, as the positive flank represents sputter removal of the frozen water initially covering the globule and the negative flank represents sputter removal of the fat globule itself. However, further studies are needed to clarify the extent to which the measured sputter yield can be associated with the sputter yield of frozen water.

3.4. Triglyceride composition in emulsions using ToF-SIMS

The fatty acid composition of the triglycerides was investigated and compared between the samples by extracting mass spectra from ROIs corresponding to fat-rich parts of the ion images. Analysis of triglycerides with ToF-SIMS is known to produce positive diacylglycerol (DAG) ions at relatively high yields, i.e., an ionized triglyceride molecule after detachment of one fatty acid during then primary ion collision process (Debois et al., 2009). Thus, Fig. 7a displays mass spectra of fat-rich ROIs in a mass range that includes peaks corresponding to a large variety of DAG ions, DAG X:Y, where X and Y denote the total number of carbon atoms and double bonds, respectively, in the two fatty acids of the DAG ion.

In Fig. 7b, the distribution of DAG X:Y peak intensities in the mass spectra are displayed for the three samples, also including monoacyl glycerol (MAG X:Y) ions (triglyceride fragments after ion-collision-induced loss of two fatty acids). Similar DAG/MAG distributions are observed for bovine milk and cream, including considerable contributions from a broad range of DAG ions, from DAG18:0 to DAG36:2, whereas that for the oat-based cream analogue is distinctly different, with dominating contributions from DAG 36:2-4 and, to a lesser extent, DAG 34:1-2. The former distributions are consistent with the reported fatty acid distribution in Swedish cow milk (Mansson, 2008), in which the major fatty acids are C16:0 (30.6%), C18:1 (22.8%), C18:0 (12.2%), and C14:0 (10.9%), but with significant contributions also from C4:0 (4.4%), C6:0 (2.4%), C10:0 (2.7%), and C12:0 (3.3%). In addition, quantitative agreement with the reported fatty acid distribution was

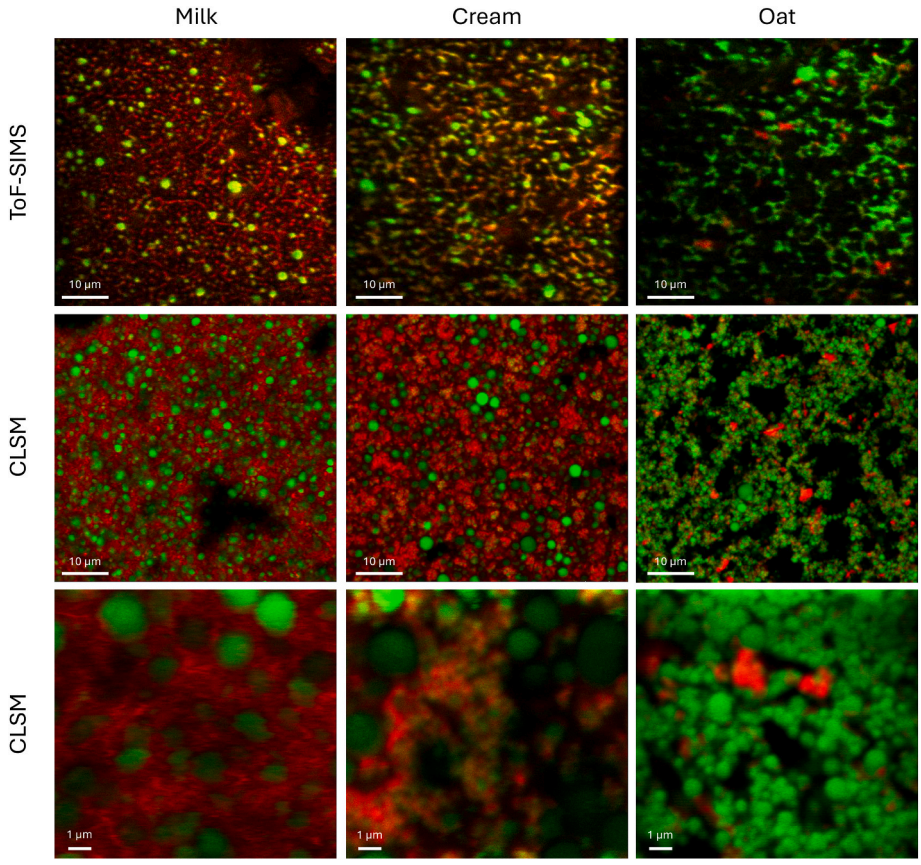

Fig. 4. Comparison of ToF-SIMS and CLSM images of the three samples. ToF-SIMS images show proteins in red and fat in green (ions as in Fig. 3) and CLSM images show proteins and sugars in red and fat in green.

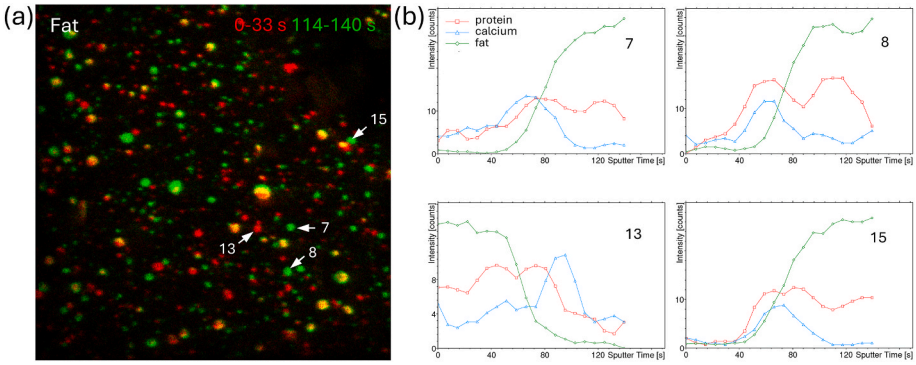

Fig. 5. 3D characterisation of fat droplets in milk emulsion. (a) Combined overlay ion image of fat accumulated at the beginning of the measurement in red (sputter time 0-33 s) and at the end of the measurement in green (114-140 s). Field of view 60 x 60 µm^2. (b) Depth profiles of fat (green, $C_5H_7^+ + C_5H_9^+ + C_6H_8^+ + C_6H_9^+ + C_6H_{11}^+ + C_7H_9^+ + C_7H_{11}^+$), protein (red, $CH_4N^+ + C_2H_6N^+ + C_4H_8N^+$) and calcium (blue, $Ca^+ + CaOH^+$) in four individual fat droplets, marked in (a).

observed in a ToF-SIMS negative ion measurement of the fatty acid ion distribution in bovine milk (Supplementary Fig. S6), after correction of the peak intensities with a monotonically decreasing sensitivity factor with increasing ion mass.

The DAG/MAG distribution of the oat-based cream analogue, strongly peaked at DAG 36:2-4 and DAG 34:1-2, matches well the reported fatty acid distribution of rapeseed oil, which is dominated by C18:1 (60.7%), C18:2 (21.2%), and C18:3 (11.8%), with only minor fractions of the saturated fatty acids C16:0 (4.8%) and C18:0 (1.5%) (Dupain et al., 2007). Furthermore, the large fractions of C18:1 and C18:2 in rapeseed oil are reflected in the high signal intensities of MAG18:1 and MAG18:2 for the oat-based cream analogue sample.

3.5. Imaging of emulsions at the nanometer scale using TEM

Fig. 8 shows TEM images of milk, cream, and oat-based cream analogue at two different magnifications. For milk, the TEM images display circular structures in the 0.5-1 µm size range, isolated and randomly distributed in the emulsion, consistent with fat globules. The bright portion in most of the circular structures indicates that the triglyceride content of the fat droplets was partially exchanged during the plastic embedding process, although the fat droplet membrane can still be seen. Between the fat globules, a mixture of distinct dark round structures, about 100 nm in size, and lighter grey structures of similar size, as well as elongated grey structures can be observed. The distinct dark round structures with a size of approximately 100 nm are

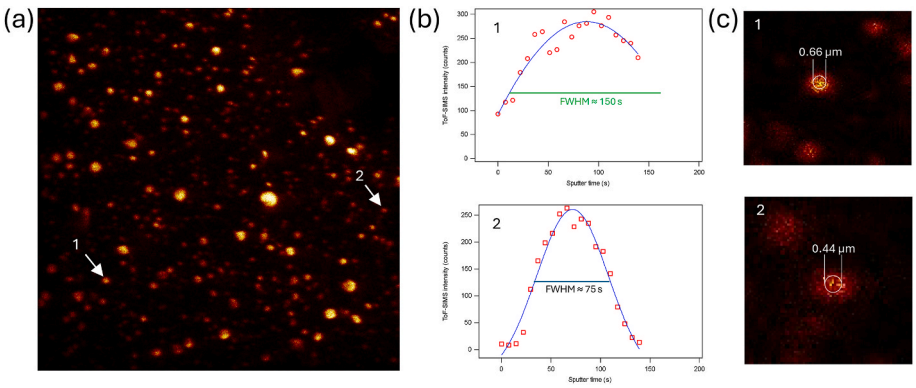

Fig. 6. Determination of sputter yield from 3D measurements of fat droplets in milk emulsion. (a) Ion image of fat globules in milk (field of view 60 × 60 µm^2), (b) depth profiles of the two individual fat droplets marked in (a) and (c) magnified images of the two fat droplets (from (a)) showing the manually estimated globule diameters.

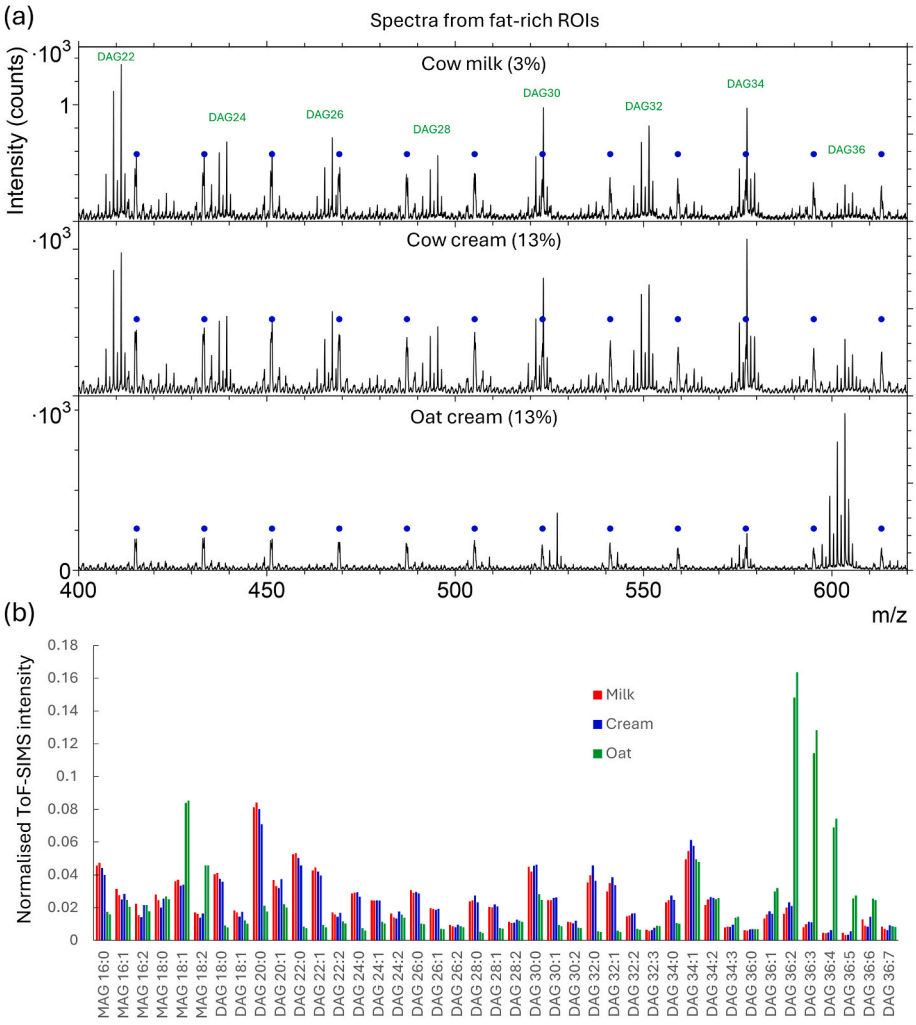

Fig. 7. Distribution of DAG and MAG ions in mass spectra of fat-rich ROIs from milk, cream and oat-based cream analogue. (a) Mass spectra in a m/z range displaying peaks assigned to DAG ions. Groups of DAG ions with different number of carbon atoms are indicated, where each group include peaks for different number of double bonds. Blue dots indicate water cluster peaks. (b) ToF-SIMS peak intensity distributions for MAG and DAG ions, two measurements for each sample. The peak intensities were normalised to the added peak intensity of all included peaks.

interpreted as casein micelles (Sinaga et al., 2017), based on comparison with a cryo-TEM image of a vitrified thin film of milk (Fig. 9). While the size and external appearance of the dark round structures are similar in the two images, suggesting that they have a common origin, the cryo-TEM image (Fig. 9b) reveals distinct internal structures consistent with casein micelles, such as the homogeneous distribution of dark, small particles, which can be interpreted as calcium phosphate nanoclusters embedded in a network of β- and α_S-caseins (Acevedo-Fani et al.,

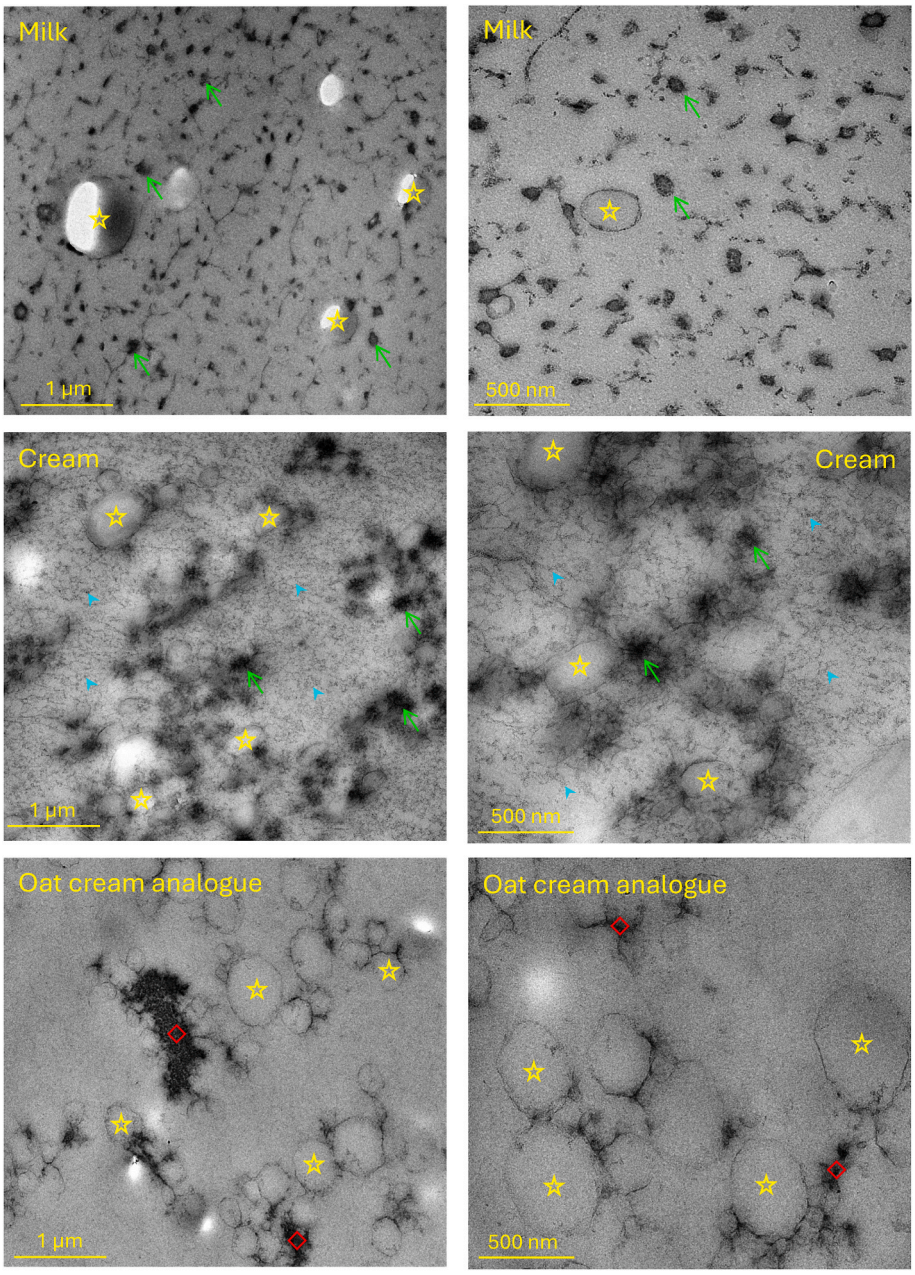

Fig. 8. TEM images comparing the three samples at two different magnifications. Yellow stars – fat droplets, green arrows – casein micelles, cyan arrowheads – whey proteins, red diamonds – proteins. The samples were prepared by freeze substitution and plastic embedding.

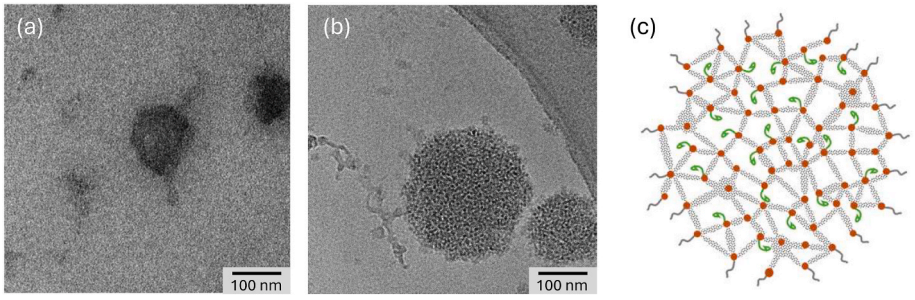

Fig. 9. TEM images of structures interpreted as casein micelles in milk prepared by (a) freeze substitution and plastic embedding, and (b) by plunge freezing and analyzed in its native state by cryo TEM. (c) Conceptual model of a casein micelle, adapted from (Dalgleish & Corredig, 2012), where the brown dots represent calcium phosphate nanoclusters, which are connected with a mix of β- and α_S-caseins, shown as grayish strands. The green strands correspond to β-caseins and the dark grey strands represent κ-caseins, which are located on the casein micelle surface.

2020), as previously suggested and schematically illustrated in Fig. 9c (Dalgleish & Corredig, 2012; de Kruif et al., 2012; Malmgren et al., 2017; McMahon & Oommen, 2008; Runthala et al., 2023). The lighter grey features in Fig. 8 are interpreted as whey proteins (Hillbrick et al., 1999).

These observations are consistent with the ToF-SIMS images of milk, including the randomly distributed fat globules and the background "network" of spot-like and elongated structures containing protein, calcium, lactose, and phospholipids. In the TEM images, the fat globules are typically surrounded by a thin, variably dark grey layer, interpreted as casein and/or whey proteins, whereas casein micelles are only occasionally in contact with the fat globules. These observations are consistent with the ToF-SIMS depth profiles showing a thin layer of calcium on the globule surface and a protein layer that also extends into the fat globule (Fig. 5b), suggesting that both whey proteins and casein are acting as emulsifying agents in milk.

In contrast to milk, the TEM images of cream display abundant small fat globules, 100-500 nm, which are aggregated and mixed with casein micelles in elongated structures (Fig. 8), indicating a seemingly more connected microstructure than in milk, built up by casein micelles and small fat droplets. The smaller grey structures interpreted as whey proteins are connecting the casein micelles and fat droplets in the aggregates and are also present as a very fine network between the aggregates. These observations are consistent with the ToF-SIMS images of cream, in which the elongated structures of mixed fat and proteins can now be assigned to elongated aggregates of small fat globules mixed with casein micelles (as observed also by CLSM, Fig. 4).

The TEM images of the oat-based cream analogue display similar elongated aggregates of small fat globules as for cream, but without structures similar to casein micelles and whey proteins. Supported by the ToF-SIMS images, the large dark structures in the TEM images are interpreted as protein aggregates. Small amounts of a similar dark material, also interpreted as proteins, are present on the surfaces of the fat globules, most likely with an emulsifying function. These images are largely consistent with the ToF-SIMS images, with fat and proteins distributed in elongated structures and proteins also as large aggregates. However, the elongated disaccharide (maltose) structures, which are separate from the elongated fat structures in the ToF-SIMS images of the oat-based cream analogue (Fig. 3), could not be identified in the TEM images.

4. Conclusions

This study demonstrates the analytical advantages and opportunities of combining cryo-ToF-SIMS with TEM and advanced cryo preparation, to reveal structural and molecular details in food emulsions at spatial resolutions down to the nanometer scale. It was shown that milk is characterized by isolated fat globules, separated by a network structure of homogeneously mixed casein, lactose, and phospholipids, whereas cream is largely made up of elongated aggregates of small fat globules mixed with casein, lactose and phospholipids, together with occasional, larger fat globules. The oat-based cream analogue contained similar elongated aggregates of small fat globules, but with considerably less correlation/mixing of the molecular components as compared to the bovine cream and milk. The surface of individual milk fat globules was characterized by molecular depth profiling, showing results consistent with the presence of casein on the globule surface and other proteins extending deeper into the globule, presumably originating from the protein-containing MFGM. Furthermore, the fatty acid composition of the triglyceride content in the fat globules was characterized by mass spectral analysis and found consistent with Swedish cow milk for bovine milk and cream and with rapeseed oil for the oat-based cream analogue. However, focused investigations with improved statistics are needed to acquire quantitative results and conclusive evidence for the observations made in this study. Cryo-ToF-SIMS is a complex method with several limitations including matrix effects, which affect signal intensities and quantification capabilities. Sample preparation is critical in ToF-SIMS, given the extreme surface sensitivity of the measurement, and the analysis of emulsions also entails the added complication of possible freezing artifacts associated with the cryo preparation.

CRediT authorship contribution statement

Peter Sjövall: Writing – review & editing, Writing – original draft, Methodology, Investigation, Formal analysis, Data curation, Conceptualization. **Annika Altskär:** Writing – review & editing, Methodology, Investigation, Formal analysis, Data curation. **Niklas Lorén:** Writing – review & editing, Methodology, Funding acquisition, Conceptualization.

Declaration of competing interest

The authors declare that they have no known competing financial interests or personal relationships that could have appeared to influence the work reported in this paper.

Acknowledgement

This research did not receive any specific grant from funding agencies in the public, commercial, or not-for-profit sector.

Appendix A. Supplementary data

Supplementary data to this article can be found online at https://doi.org/10.1016/j.lwt.2026.119660.

Data availability

Data will be made available on request.

References

Acevedo-Fani, A., Dave, A., & Singh, H. (2020). Nature-Assembled Structures for Delivery of Bioactive Compounds and Their Potential in Functional Foods. *Frontiers of Chemistry, 8*, 564021. https://doi.org/10.3389/fchem.2020.564021

Adler, J., & Parmryd, I. (2010). Quantifying colocalization by correlation: The Pearson correlation coefficient is superior to the Mander's overlap coefficient. *Cytometry, Part A, 77*(8), 733–742. https://doi.org/10.1002/cyto.a.20896

Brison, J., Robinson, M. A., Benoit, D. S., Muramoto, S., Stayton, P. S., & Castner, D. G. (2013). TOF-SIMS 3D imaging of native and non-native species within HeLa cells. *Analytical Chemistry, 85*(22), 10869–10877. https://doi.org/10.1021/ac402288d

Dalgleish, D. G., & Corredig, M. (2012). The structure of the casein micelle of milk and its changes during processing. *Annual Review of Food Science and Technology, 3*, 449–467. https://doi.org/10.1146/annurev-food-022811-101214

de Kruif, C. G., Huppertz, T., Urban, V. S., & Petukhov, A. V. (2012). Casein micelles and their internal structure. *Advances in Colloid and Interface Science, 171–172*, 36–52. https://doi.org/10.1016/j.cis.2012.01.002

Debois, D., Bralet, M. P., Le Naour, F., Brunelle, A., & Laprevote, O. (2009). In situ lipidomic analysis of nonalcoholic fatty liver by cluster TOF-SIMS imaging. *Analytical Chemistry, 81*(8), 2823–2831. https://doi.org/10.1021/ac900045m

Dupain, X., Costa, D. J., Schaverien, C. J., Makkee, M., & Moulijn, J. A. (2007). Cracking of a rapeseed vegetable oil under realistic FCC conditions. *Applied Catalysis B: Environmental, 72*(1), 44–61. https://doi.org/10.1016/j.apcatb.2006.10.005

German, J. B., & Dillard, C. J. (2006). Composition, structure and absorption of milk lipids: A source of energy, fat-soluble nutrients and bioactive molecules. *Critical Reviews in Food Science and Nutrition, 46*(1), 57–92. https://doi.org/10.1080/10408690590957098

Hillbrick, G. C., McMahon, D. J., & McManus, W. R. (1999). Microstructure of indirectly and directly heated ultra-high-temperature (UHT) processed milk examined using transmission electron microscopy and immunogold labelling. *LWT - Food Science and Technology, 32*(8), 486–494. https://doi.org/10.1006/fstl.1999.0586

Horne, D. S. (2020). Chapter 6 - Casein micelle structure and stability. In M. Boland, & H. Singh (Eds.), *Milk proteins* (3rd ed., pp. 213–250). Academic Press.

Jia, F., Zhao, X., & Zhao, Y. (2023). Advancements in ToF-SIMS imaging for life sciences. *Frontiers of Chemistry, 11*, Article 1237408. https://doi.org/10.3389/fchem.2023.1237408

Jukkola, A., & Rojas, O. J. (2017). Milk fat globules and associated membranes: Colloidal properties and processing effects. *Advances in Colloid and Interface Science, 245*, 92–101. https://doi.org/10.1016/j.cis.2017.04.010

Kupikowska-Stobba, B., Domagała, J., & Kasprzak, M. M. (2024). Critical review of techniques for food emulsion characterization. *Applied Sciences, 14*(3), 1069.

Lapcikova, B., Lapcik, L., Valenta, T., & Chvatikova, M. (2024). Plant-Based emulsions as dairy cream alternatives: Comparison of viscoelastic properties and colloidal stability of various model products. *Foods, 13*(8). https://doi.org/10.3390/foods13081225

Lara-Villoslada, F., Olivares, M., & Xaus, J. (2005). The balance between caseins and whey proteins in cow's milk determines its allergenicity. *Journal of Dairy Science, 88*(5), 1654–1660. https://doi.org/10.3168/jds.S0022-0302(05)72837-X

Li, R., Peng, S., Zhang, R., Dai, T., Fu, G., Wan, Y., … McClements, D. J. (2019). Formation and characterization of oil-in-water emulsions stabilized by polyphenol-polysaccharide complexes: Tannic acid and β-glucan. *Food Research International, 123*, 266–275. https://doi.org/10.1016/j.foodres.2019.05.005

Malmgren, B., Ardö, Y., Langton, M., Altskär, A., Bremer, M. G. E. G., Dejmek, P., & Paulsson, M. (2017). Changes in proteins, physical stability and structure in directly heated UHT milk during storage at different temperatures. *International Dairy Journal, 71*, 60–75. https://doi.org/10.1016/j.idairyj.2017.03.002

Mansson, H. L. (2008). Fatty acids in bovine milk fat. *Food & Nutrition Research, 52*. https://doi.org/10.3402/fnr.v52i0.1821

McClements, D. J. (2015). *Food emulsions: Principles, practices, and techniques* (3rd ed.). Boca Raton: CRC Press.

McMahon, D. J., & Oommen, B. S. (2008). Supramolecular structure of the casein micelle. *Journal of Dairy Science, 91*(5), 1709–1721. https://doi.org/10.3168/jds.2007-0819

O'Callaghan, T. F., McCarthy, E. K., & Carey, C. C. (2025). Milk fat globule membrane ingredients and their potential applications for human health and performance. *Current Opinion in Food Science, 63*, Article 101302. https://doi.org/10.1016/j.cofs.2025.101302

Parlanti, P., & Cappello, V. (2022). Microscopes, tools, probes, and protocols: A guide in the route of correlative microscopy for biomedical investigation. *Micron, 152*, Article 103182. https://doi.org/10.1016/j.micron.2021.103182

Pawley, J. B. (2006). *Handbook of biological confocal microscopy* (3 ed.). New York, NY: Springer.

Rabbani, A., Ayyash, M., D'Costa, C. D. C., Chen, G., Xu, Y., & Kamal-Eldin, A. (2025). Effect of heat pasteurization and sterilization on milk safety, composition, sensory properties, and nutritional quality. *Foods, 14*(8). https://doi.org/10.3390/foods14081342

Ravera, F., Dziza, K., Santini, E., Cristofolini, L., & Liggieri, L. (2021). Emulsification and emulsion stability: The role of the interfacial properties. *Advances in Colloid and Interface Science, 288*, Article 102344. https://doi.org/10.1016/j.cis.2020.102344

Runthala, A., Mbye, M., Ayyash, M., Xu, Y., & Kamal-Eldin, A. (2023). Caseins: Versatility of their micellar Organization in relation to the functional and nutritional properties of milk. *Molecules, 28*(5). https://doi.org/10.3390/molecules28052023

Seah, M. P. (2015). Argon cluster size-dependence of sputtering yields of polymers: Molecular weights and the universal equation. *Surface and Interface Analysis, 47*(1), 169–172. https://doi.org/10.1002/sia.5656

Sinaga, H., Bansal, N., & Bhandari, B. (2017). Effects of milk pH alteration on casein micelle size and gelation properties of milk. *International Journal of Food Properties, 20*(1), 179–197. https://doi.org/10.1080/10942912.2016.1152480

Sjovall, P., Gregoire, S., Wargniez, W., Skedung, L., Detroyer, A., & Luengo, G. S. (2024). Spatial distribution of active compounds in stratum corneum-partitioning between corneocytes and lipid matrix. *Scientific Reports, 14*(1), Article 18681. https://doi.org/10.1038/s41598-024-66418-x

Starr, N. J., Khan, M. H., Edney, M. K., Trindade, G. F., Kern, S., Pirkl, A., … Scurr, D. J. (2022). Elucidating the molecular landscape of the stratum corneum. *Proceedings of the National Academy of Sciences of the United States of America, 119*(12), Article e2114380119. https://doi.org/10.1073/pnas.2114380119

Tan, C., & McClements, D. J. (2021). Application of advanced emulsion technology in the food industry: A review and critical evaluation. *Foods, 10*(4). https://doi.org/10.3390/foods10040812

Yu, Y., Li, X., Zhang, J., Li, X., Wang, J., & Sun, B. (2023). Oat milk analogue versus traditional milk: Comprehensive evaluation of scientific evidence for processing techniques and health effects. *Food Chemistry X, 19*, Article 100859. https://doi.org/10.1016/j.fochx.2023.100859

Zhang, J., Brown, J., Scurr, D. J., Bullen, A., MacLellan-Gibson, K., Williams, P., … Rakowska, P. D. (2020). Cryo-OrbiSIMS for 3D molecular imaging of a bacterial biofilm in its native State. *Analytical Chemistry, 92*(13), 9008–9015. https://doi.org/10.1021/acs.analchem.0c01125

Zhou, X., Sala, G., & Sagis, L. M. C. (2022). Structure and rheological properties of oil-water and air-water interfaces stabilized with micellar casein isolate and whey protein isolate mixtures. *Food Hydrocolloids, 133*, Article 107946. https://doi.org/10.1016/j.foodhyd.2022.107946

Zuber, B., & Lucic, V. (2019). Molecular architecture of the presynaptic terminal. *Current Opinion in Structural Biology, 54*, 129–138. https://doi.org/10.1016/j.sbi.2019.01.008